ACS APPLIED MATERIALS & INTERFACES

Research Article

www.acsami.org

# Redox Active Polymer Brushes with Phenothiazine Moieties

Ali A. Golriz,[†,‡] Tassilo Kaule,[†] Maria B. Untch,[†] Krzysztof Kolman,[⊥] Rüdiger Berger,[†] and Jochen S. Gutmann*[,‡,§]

[†]Max Planck Institute for Polymer Research, Ackermannweg 10, D-55128 Mainz, Germany

[‡]Department of Chemistry and Center for Nanointegration Duisburg-Essen (CENIDE), University Duisburg-Essen, Universitätsstr. 5, D-45117 Essen, Germany

[§]Deutsches Textilforschungszentrum Nord-West e.V., Adlerstr. 1, D-47798 Krefeld, Germany

[⊥]Polymer Technology and Engineering Division, Wroclaw University of Technology, Wybrzeze Wyspianskiego 27, 50-370 Wrocław, Poland

Supporting Information

**ABSTRACT:** We have investigated two different concepts to synthesize redox active polymer brushes using surface initiated atomic transfer radical polymerization (SI-ATRP). This polymerization technique allows the synthesis of well-defined grafted polymer brushes. In the initial step the surface was functionalized with a self-assembling monolayer of the SI-ATRP starter. Then, polymer brushes carrying phenothiazine moieties were grafted from the surface via SI-ATRP. The first concept consists of polymerizing monomers with phenothiazine pendant moieties to directly incorporate the redox functionality as side group in the growing polymer brush. The second concept consists of using grafted activated ester brushes which are functionalized with phenothiazine redox moieties in a successive reaction step. The electrochemical properties of the grafted redox active brushes were examined by cyclic voltammetry. Furthermore, the surface morphology and the chemical composition of the polymer brushes were characterized using scanning force microscopy (SFM), X-ray techniques, and UV/vis spectroscopy. Apart from their redox behavior, the synthesized brushes revealed increased mechanical stability on the nanoscale.

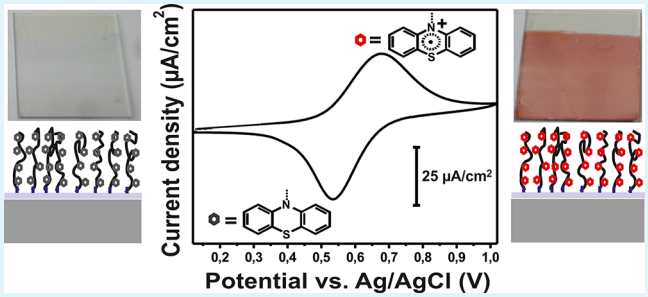


**KEYWORDS:** *polymer brushes, redox active, phenothiazine, activated ester, SI-ATRP, postfunctionalization*

## INTRODUCTION

Polymers with redox active properties are interesting materials for the electronic industry. The cheap production costs as well as the easy processing make these polymers attractive components for application in electronic devices such as solar cells and organic memory devices (OMDs)[1] as well as polymer based batteries.[2] Due to their organic nature, redox active polymers in many cases face problems of incompatibility with inorganic substrates during the processing. In some cases, spin-cast processes lead to a dewetting behavior of the polymer film.[3] The dewetting often results in formation of agglomerates and rough surfaces.[4] To prevent dewetting and increase the homogeneity of the polymer layer films, chemical surface functionalization can serve as an alternative method.[5] Polymer chains can be attached to the substrate surface by means of chemical grafting techniques.[6,7] Grafted polymers have a confined geometry because of their covalent bonding and therefore cannot dewet from the surface when their grafting density exceeds a certain limit.[8] If polymer chains are forced to stretch[9] and their surface area density is sufficiently high, they will form so-called "brush like" structures.[10] A great advantage of grafted polymer brushes is their high mechanical stability. Especially on the nanometer scale, scanning force microscopy (SFM) based nanowear experiments showed that covalently bound polymer brushes exhibit an increased mechanical nanowear behavior compared to spin coated polymer films.[11,12] Grafted polymer brushes possess increased elastic moduli and plasticity which stem from the entropic effect lowering the stress contribution.[13] This increased mechanical stability is a very important feature for polymers in the electronic industry.[14−16] Grafted redox polymer brushes[17] can be used as cathode active materials in organic radical batteries.[18,19] The grafting prevents dissolution of the organic electrode material[20] which until now is mainly achieved by cross-linking of the polymer network.[21,22] The cross-linking has an effect on the diffusion processes taking place in the electrode material. Kojima et al. used cross-linked poly(vinylferrocene-co-*N*-vinylcarbazole) to influence the charge transfer rate on glassy carbon.[23] An alternative to cross-linking is presented by grafting techniques. Recently, Wang et al. synthesized redox active

Received: November 27, 2012
Accepted: February 13, 2013
Published: February 13, 2013

 © 2013 American Chemical Society 

polymer thin films from poly(2,2,6,6-tetramethyl-piperidin-1-oxyl-4-yl methacrylate), PTMA.[24] They used the micro contact printing method to graft PTMA brushes on flexible indium tin oxide (ITO) substrates by the surface initiated atomic transfer radical polymerization (SI-ATRP) technique.[25] This polymerization technique is chemically versatile, tolerant against impurities, water, aliphatic alcohols, and other polar solvents as well as insensitive to traces of oxygen.[26] In comparison to other controlled radical polymerization methods such as reversible-addition fragmentation chain transfer (RAFT), ATRP allows one to alter the order of addition of monomers inside a sequential block copolymer by monomer reactivity. This unique advantage leads to increased freedom in designing polymer architecture. With this technique, a broad variety of polymers with different functional groups can be grown on the surface by either the grafting to or grafting from approach.[27] With the latter SI-ATRP technique, polymer film thickness, architecture, and composition can be controlled very precisely. Another advantage is that the initiators necessary for this grafting technique are either commercially available or can be accessed via a relatively easy synthetic route.[27,28] SI-ATRP can be used to synthesize surfaces with functional groups like activated esters.[27,29−31] Polymer brushes with activated ester groups on each repetition unit have been reported for reactive surface coating.[27,32,33] Through formation of stable amide bonds, organic moieties with primary or secondary amine groups can chemically be attached to the activated ester side groups in the polymer chain. The attachment takes place quantitatively without the use of catalyst under mild reaction conditions.[34]

In a previous study, we showed the nanopatterning of spin coated poly-3-vinylbenzylphenothaizine (PVBPT) on gold using conductive SFM.[35] This polymer contains phenothiazine redox moieties on each repetition unit. Phenothiazine shows two reversible oxidation steps with relatively high electron exchange rate.[36,37] The ability to undergo $\pi-\pi$-stacking[38] makes phenothiazine and phenothiazine based polymers[39,40] interesting materials with respect to their conductivity, their redox behavior, and their electric properties. Thus, PVBPT can be regarded as an adequate candidate for data storage applications. Due to formation of stable radical cation species by oxidation, patterns with different conductivity could be stored in the polymer film for at least several days. In this study, we focused on synthesizing grafted redox active polymer brushes with phenothiazine moieties, which should exhibit a better mechanical stability regarding the surface wear compared to spin coated polymer film. For this purpose, two different synthetic routes were tested (Scheme 1). For the first route, we simply functionalized a conductive substrate like indium tin oxide (ITO) with a SI-ATRP initiator (direct polymerization). Then, we polymerized directly a monomer containing redox active phenothiazine moieties via grafting from polymerization. For the second route, we first used SI-ATRP to polymerize a monomer with functional activated ester groups. In a second step, this functional polymer was then postfunctionalized with different redox moieties based on phenothiazine. We chose two different redox moieties with one and two amine functionalities. The moiety with two amine groups can form cross-linked structures, whereas the moiety with a single amine group cannot build cross-linked bounds.

**Scheme 1. Schematic Overview of the Phenothiazine Based Redox Polymer Synthesis[a]**

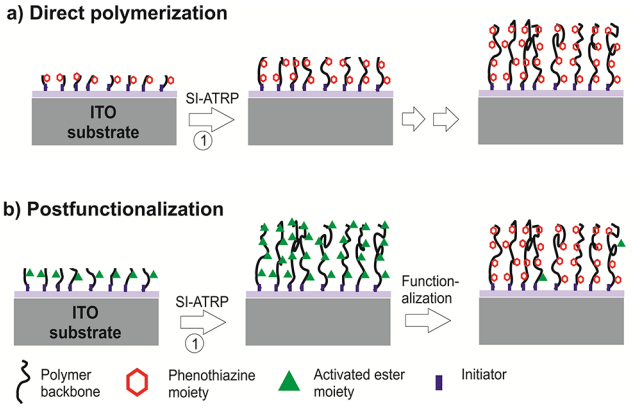


[a](a) For the first synthetic route, the phenothiazine containing polymer PVBPT was grafted from ITO substrate via SI-ATRP. (b) For the second synthetic route, polymers with activated ester moieties were grafted from ITO via SI-ATRP. Finally, these brushes were postfunctionalized with phenothiazine redox moieties.

## EXPERIMENTAL SECTION

**Methods.** The cyclic voltammetry (CV) measurements were performed with the potentiostat Autolab PGSTAT 100 from Metrohm in a modified cell equipped with a stirrer and a nitrogen supply valve. A 0.1 M solution of tetrabutylammonium perchlorate in dry dichloromethane (DCM) or acetonitrile (ACN) served as an electrolyte solution. ITO substrates with grafted polymers were used as the working electrode, and a platinum wire was used as the counter electrode, respectively. As reference, an Ag/AgCl electrode was chosen. The formal potential of the ferrocene/ferrocenium redox couple was determined to be 0.44 V versus this reference electrode.

UV/vis spectra were recorded on a Perkin-Elmer Lambda-9 with ITO substrate as the background standard. For the CV measurements and the X-ray reflectivity (XRR) measurements, ITO substrates on glass as well as silicon substrate were prepared by the following procedure: Glass slides (2.5 cm × 2.5 cm × 0.5 cm) and silicon substrate (Si-Mat, one side polished, 2.5 cm × 2.5 cm × 0.54 cm) were cut using a glass cutter and sonicated for 10 min subsequently with DCM, acetone, and Alconox and washed with Milli-Q water. Finally, the glass slides and the silicon substrate were dried with compressed air and dried at 100 °C in vacuum. On the glass slides, 100 nm of ITO was sputtered under argon flow. The ITO sputtered glass slides and the silicon substrates were cleaned with DCM, dried under air, and cut in 1.1 cm × 1.1 cm slices.

XRR measurements on substrates were performed on a XRD 3003 TT, Seifert Ltd. GB diffraction system. Monochromatic and collimated X-rays were obtained from a copper anode with a wavelength of $\lambda$ = 0.154 nm. Herein, the thickness was determined according to parratt formalism.[41] Contact angle measurements were conducted on a Krüss, DSA10-MK2.

X-ray photoelectron spectroscopy (XPS) measurements were performed on a SPECS Surface Nano Analysis machine using Al K$\alpha$ radiation. The incidence angle of X-rays was 45° with respect to surface normal. All the measurements by XPS were performed at pressures lower than $3 \times 10^{-9}$ mbar. The peak area was calculated from the integrals using OriginPro 8.0 software after correction by individual peak sensitivity given by the SPECS manual instruction. For the AE brushes, the oxygen peak of the $SiO_2$ layer underneath was subtracted before calculation.

The nanowear experiments were carried out on a NanoWizard scanning force probe microscope (JPK, Berlin, Germany) using contact mode cantilevers (NanoWorld, CONT-W, nominal spring constant 0.2 N/m). The exact spring constant for each cantilever was determined by thermal tune. A surface of $3 \times 3$ $\mu m^2$ was scanned 100

Scheme 2. SI-ATRP Using Silane Starter with Bromoisobutyrate Functionality on Si/ITO Surface

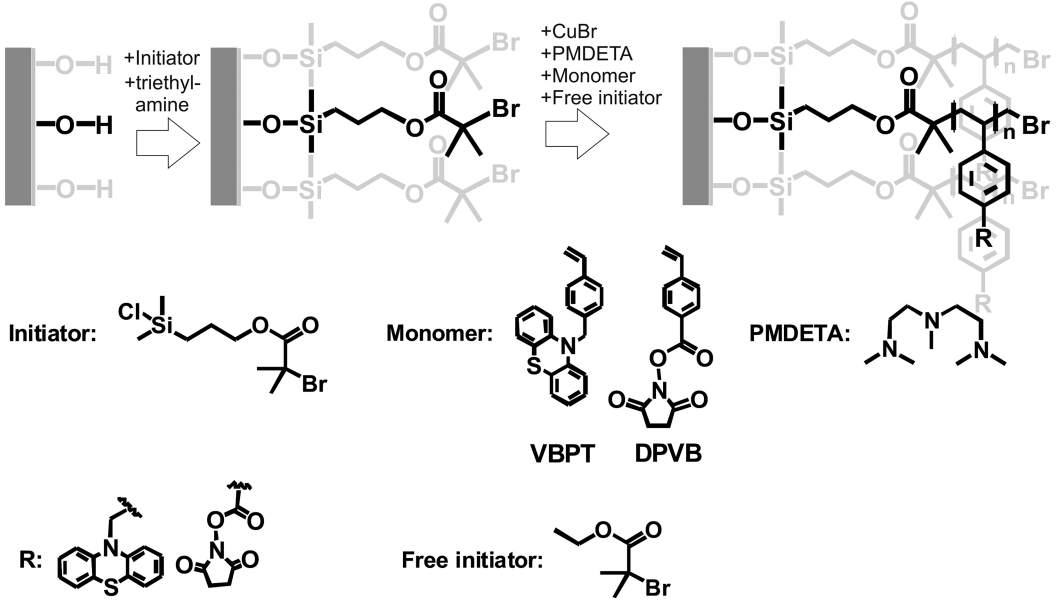


times in contact mode with a load of 10 nN at a speed of 50 $\mu$m/s. Then, the scanned area was mapped in tapping mode to observe changes in the topography.[11]

**Materials and Synthesis.** Used materials and the synthetic approach of grafted poly 10-(4-vinylbenzyl)-10H-phenothiazine (PVBPT) brushes via SI-ATRP as well as the activated ester brushes poly 2,5-di oxopyrrolidin-1-yl4-vinylbenzoate (PDPVB) and their functionalization are described in the Supporting Information.

## RESULTS AND DISCUSSION

**Direct Polymerization.** We attached PVBPT to substrates by a grafting from polymerization. For this purpose, silicon and ITO surfaces were functionalized with an ATRP silane starter. 4-Vinylbenzylpheonthiazine (VBPT) was used for surface polymerization (Scheme 2).

XRR measurements were performed to obtain thickness and root mean square (RMS) roughness of the polymer brush films (Supporting Information, Figure S 1 and Table T 1). Simultaneously, using free sacrificial initiator, we were able to determine the molecular weight of the free polymer and its distribution by size exclusion chromatography (SEC). The molecular weight $M_n$ obtained from the SEC could be related with the polymer brush film thickness (Supporting Information, Figure S 2). With increasing molecular weight $M_n$ of the free polymer from 5700 to 22 400 g/mol, we observed a linear increase of the thickness $d$ from 4.8 ± 0.5 to 11.3 ± 1.3 nm. The intercept of the line is at 1.8 ± 1.2 nm, which is close to zero as expected for SI-ATRP (Supporting Information, Figure S 2).[58]

In addition, a grafting density of $\sigma_{Exp}$ = 0.31 ± 0.11 chains/nm$^2$ was calculated from the fitted XRR data (with a polymer density of $\rho$ = 1.01 g/cm$^3$, $M_n$ = 22 400 g/mol) using the eq 1.

$$\sigma_{Exp} = \frac{d \times \rho}{M_n} \quad (1)$$

This value is in good accordance with the value provided from the literature for grafted polystyrene (PS) or poly(methylmethacrylate) (PMMA).[58,42] For grafted PS brushes, a value of $\sigma_{Exp}$ = 0.44 chains/nm$^2$ was reported. For PVBPT brush, we could calculate a theoretical maximum interchain distance of $a$ = 1.49 nm using the eq 2.

$$a = \sqrt{\frac{1.41 \times M}{100 \times n}} \quad (2)$$

This equation was used by Privalko et al. to estimate cross-sectional areas of different polymer chains.[43] Here, we estimated helical conformation with a $HC_1$ geometry of the polymer chains with $M$ = molecular weight of the repeating unit (315.42 g/mol) and $n$ = number of main-chain bonds in the chain repeating unit (in our case $n$ = 2).[43] The estimation of a helical structure is justified for bulky polymers such as poly(vinyl carbazole) which have an interchain distance of around 1.2 nm.[44] Molecular dynamic simulation of the PVBPT brush grafted from silicon substrate revealed short-range and wide-range helical domains (Supporting Information, Figure S 3). A theoretical grafting density of $\sigma_{Theo} = 1/a^2$ = 0.45 chains/nm$^2$ was calculated which represents the maximum theoretical grafting density for PVBPT grafted brushes. A further proof for the successful reaction was obtained from the static contact angle. The average contact angle of the surface grafted PVBPT was measured to be around 86 ± 3° regardless of the molecular weight (Supporting Information, Figure S 4). In comparison, the ITO layer functionalized with the initiator showed a static contact angle of around 70 ± 4°. The increase in contact angle by 17 ± 4° indicates that polymerization has taken place successfully on the surface (Supporting Information, Table T 1 and Figure S 4).

**Redox Functionality of PVBPT Grafted Brushes.** In order to prove the redox activity of the PVBPT brushes, cyclic voltammetry (CV) measurement of the polymers grafted on ITO substrates were performed (Figure 1). In the first experiment, a solution of PVBPT in DCM was measured against ITO as working electrode. For the PVBPT in solution, we found an anodic oxidation peak of $E_0^{0/+1}$ = 0.66 V and a cathodic reduction peak of $E_0^{+1/0}$ = 0.57 V at a scan speed of 10 mV/s (Supporting Information, Figure S 5). For the initiator functionalized ITO substrate, we did not observe any oxidation peaks. For the grafted PVBPT brushes ($M_n$ = 22 400 g/mol, $d$ =

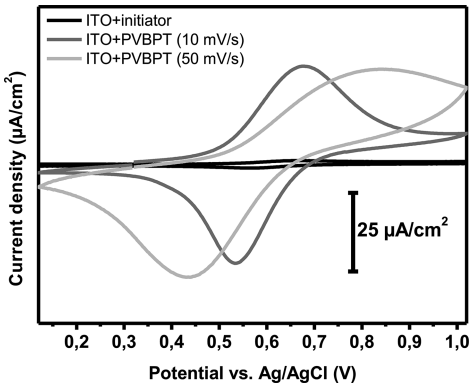


**Figure 1.** Cyclic voltammetry of grafted PVBPT ($M_n$ = 22 400 g/mol, $d$ = 11.3 nm) on ITO substrates at different scan speed in 0.1 M tetrabutylammonium perchlorate/DCM solution. The potential is measured with ITO, Ag/AgCl, and Pt as the working, the reference, and the counter electrode, respectively.

11.3 nm), the CV diagrams revealed an anodic oxidation peak of $E_0^{0/+1}$ = 0.68 V and a cathodic reduction peak of $E_0^{+1/0}$ = 0.54 V at a scan speed of 10 mV/s. The shift of the oxidation potential of the polymer films compared to the solution might result from the overpotential of the polymer brush film on ITO. Morishima and co-workers stated for spin coated films of the phenothiazine polymer poly(3-vinyl-l0-methylphenothiazine) or PVMPT on platinum that overpotential occurs due to the low conductivity of the polymer film.[45] Especially for PVMPT films with high surface coverage of the electrode, the overpotential is increased with increasing scan speed. Morishima et al. observed an increase of the anoodic oxidation peak from approximately $E_0^{0/+1}$ = ~0.65 V to $E_0^{0/+1}$ = ~0.80 V when the scan speed was increased from 20 to 200 mV/s for spin coated PVMPT films on platinum (with a surface coverage of 0.29 $\mu$mol/cm$^2$). Simultaneously, the cathodic reduction peak decreased from $E_0^{+1/0}$ = ~ 0.54 V to $E_0^{+1/0}$ = ~ 0.42 V. This means that the peak separation increased from approximately $\Delta E_0$= 0.12 V to $\Delta E_0$ = 0.38 V at increasing scan speed. This shift occurs due to the aggravated diffusion through the polymer film.[45] In the case of grafted PVBPT, we observed a similar behavior when the scan speed was increased. With an increase of the scan speed from 10 mV/s to 50 mV/s, the anodic oxidation peak changed from $E_0^{0/+1}$ = 0.68 V to approximately $E_0^{0/+1}$ = 0.83 V, respectively. Simultaneously, the cathodic reduction peak decreased from $E_0^{+1/0}$ = 0.54 V to $E_0^{+1/0}$ = 0.43 V, respectively. This means the peak separation between the anodic and cathodic peak increased from $\Delta E_0$ = 0.14 V to $\Delta E_0$ = 0.40 V at increasing scan speed. The peak separation of the voltammograms at increased scan speed can be explained by diffusion behavior which leads to rather broader peaks and diffusion tails. This broadening is a further hint that overpotential plays an important role in the case of grafted PVBPT.

From the XRR data, we obtained information about the surface RMS roughness. The roughness varied between 0.8 and 1.1 nm and was independent of the molecular weight (Supporting Information, Table T 1). However, according to the SEC results, the polydispersity of the free polymer increased from 1.4 to 2.3 when the molecular weight $M_n$ increased from 5700 to 22 400 g/mol (Supporting Information, Table T 1). This indicates that the ATRP polymerization reaction becomes less controlled at higher molecular weights. The lack of control in the polymerization reaction might influence the surface morphology. Therefore, in the next step, surface morphology was characterized more in detail.

**Surface Analysis of PVBPT Brushes.** SFM experiments were performed to examine the surface morphology of the PVBPT grafted surfaces (Figure 2). Large agglomerates were

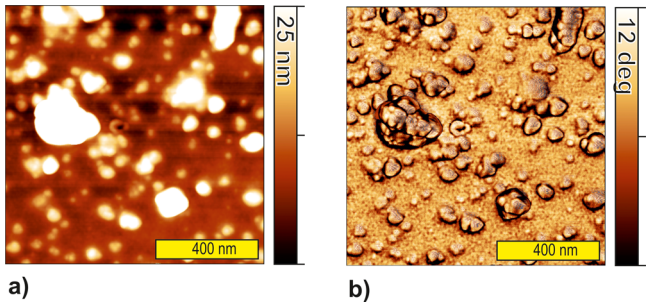


**Figure 2.** SFM image of (a) topography and (b) phase for PVBPT grafted brushes on ITO substrate ($M_n$: 22 400, $d$ = 11.3).

formed on the top of the polymer brush film with diameters varying between 20 and 300 nm. These agglomerates could not be removed by extraction or treatment in an ultrasonic bath. From the phase image, we could see that the regions with higher topography correspond to a slight increase of the phase shift in the order of 1−2°. This contrast was quite low and indicates that the agglomerates most probably consist of the same material as the polymer. Topography images also revealed the formation of larger agglomerates on the surface regardless of the molecular weight (Supporting Information, Figure S 6). The RMS roughness resulting from the SFM measurements was between 8.8 and 22.4 nm (Supporting Information, Table T 1).

To examine the origin and the chemical composition of the formed agglomerates, we conducted XPS measurements. The measurements revealed ratios between carbon, sulfur, and nitrogen atoms corresponding to the molecular formula of the grafted PVBPT brush (Supporting Information, Figure S 7 and Table T 2). The XPS beam size of 1 mm in diameter assured that the surface analysis was representative over a large observation volume including nanoscale agglomerates. Furthermore, we could exclude that the agglomerates come from copper complex[46] used for the ATRP reaction, since no copper peak was present in the XPS spectrum. Thus, we concluded that the agglomerates must come from the polymer itself during the grafting process. With respect to the high reaction temperature, it is probable that the polymerization reaction is partially thermally initiated. The polymer chains growing uncontrollably could agglomerate because of their low solubility and attach to the surface. According to the XRR data, the polymer brush film should be a uniform film without gaps. Therefore, we could see the fringes in the XRR curves (Supporting Information, Figure S 1). The initiator with the bromoisobutyrate functionality typically forms a self-assembling monolayer (SAM) with homogeneous surface morphology.[47,48] With PS brushes grafted from the same bromoisobutyrate initiator, homogeneous surfaces were obtained with polydispersities below 1.15 without the addition of sacrificial initiator.[49] For better control of the polymerization reaction, Cu (II) salts were added as deactivating agent. In the case of PVBPT brushes, the agglomerate formation already appeared at $M_n$ below 10 000 g/mol. The presence of sacrificial initiator is

obviously not enough to form a sufficient amount of persistent radicals. The addition of Cu (II) might help to decrease the polydispersity. However, then the reaction rate will be further decreased. Thus, in conclusion, the agglomerates are probably covalently bound and must result from the polymerization step due to poor reaction control. However, for electronic functional media, more homogeneous surfaces are necessary. Agglomerates on the surface might be disturbing on the nanometer scale.

The mechanical stability of the PVBPT grafted brushes was examined using SFM based nanowear experiments on ITO. Nanowear experiments are common techniques to examine tribological behavior of materials under mechanical forces. The resulting surface wear can be attributed to different wear mechanisms.[50,51] Since the experiments can be conducted under defined force application, it is possible to draw conclusions about nanowear stability of the material. For SFM based nanowear experiments, the surface was scanned in contact mode with a defined load of 10 nN on the tip. After 100 repeated scans, the surface topography was then mapped to view morphological changes of the surface (Figure 3).

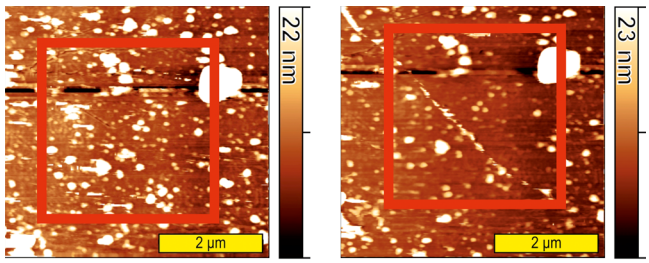


**Figure 3.** Nanowear experiment of PVBPT brushes on ITO substrate ($M_n$ = 22 400 g/mol, $d$ = 11.3 nm) at 10 nN with the speed of 50 $\mu$m/s on 3 × 3 $\mu m^2$ (red square). The topography was imaged before and after the nanowear experiment. (a) Topography image before the nanowear experiment. (b) Topography image after the nanowear experiment.

Agglomerates with diameter of 100 nm up to 1 $\mu$m were imaged on the surface before the nanowear experiment. After the nanowear experiment, we observed that the surface morphology did not change significantly. Only some of the agglomerates were displaced by the tip movement upon the surface. Apparently, many of the agglomerates were pressed or flattened into the surface making the surface smoother. According to the works of Pihan et al.,[52] particles imbedded in a polymer matrix are worn out and removed from the surface unless the particles are compatibilized with the matrix polymer by grafting a polymer brush onto particles. In our case, however, we could not observe any particles being worn out. Thus, we assume the agglomerates are not loose particles but embedded covalently on top or into the polymer film. The surface underneath the agglomerates did not reveal any topographical changes. In particular, formation of ripples and pile up at the scan edges did not occur. The RMS roughness decreased from 24 to 21 nm which confirms the mechanical stability of the grafted brushes. Under similar test conditions, spin coated PVBPT films revealed lower mechanical stability.[35] Thus, by using SI-ATRP to attach the PVBPT brushes to the substrate, we were able to increase the nanowear resistance of the surface.

**Postfunctionalization.** As an alternative route, we investigated the use of activated ester polymer brushes to obtain redox active brush polymers. Activated ester monomers are less bulky compared to VBPT and can be polymerized easily via ATRP. We examined 2,5-dioxopyrrolidin-1-yl-4-vinylbenzoate (DPVB) as the activated ester monomer.[53] First, the monomers were polymerized from the substrate via SI-ATRP (Scheme 2). Then, in a second step, the activated ester groups were replaced by phenothiazine based moieties. To functionalize the brushes, we used two different moieties (Scheme 3). The first moiety is a primary amine derivative called (10-methyl-10H-phenothiazin-3-yl)methanamine (MPMA) which was synthesized from 10-methyl-10H phenothiazine. The second moiety is new methylene blue (NMB) which is a commercially available dye. It is mainly used as staining and contrast agent for cell biology.[54] MPMA only contains one primary amine group and should not lead to cross-linking by the reaction with the activated ester groups. NMB however has two secondary amine groups and can therefore bind with the activated ester brush by cross-linking. The additional cross-linking could further mechanically stabilize the polymer film coating.[11]

Vinyl benzoates monomers are known to be easily polymerized via ATRP with high reaction rates.[55,56] To obtain the activated ester polymer brushes, again we used SI-ATRP as shown in Scheme 2. The synthesis was done according to Orski et al.[57] with the addition of sacrificial initiator in DMF to control the film thickness. Subsequently, film thickness and RMS roughness were measured with XRR (Supporting Information, Figure S 8 and Table T 3). In addition, the molecular weight of the free activated ester polymer in the reaction solution was determined by SEC. We could observe a linear dependence of the grafted polymer film thickness with increasing $M_n$ (Supporting Information, Figure S 9). The linear fit has an intercept point at approximately 0.3 ± 0.7 nm, as expected for SI-ATRP.[58] The XRR data indicate that larger film thicknesses of around 30 nm can be obtained using DPVB as monomer (Supporting Information, Table T 3).

For the PDPVB brushes, in the following referred to as AE brush, a grafting density of $\sigma_{Exp}$ = 0.36 ± 0.02 chains/nm$^2$ was obtained from the simulation of the XRR curves with eq 1. For the calculation, we used a density of $\rho$ = 1.08 g/cm$^3$ for the polymer and $M_n$ = 55 300 g/mol. For PDPVB brushes, we calculated a theoretical maximum interchain distance of $a$ = 1.31 nm using eq 2. Here, we estimated a helical conformation of the polymer chains with $M$ = molecular weight of the repeating unit (245.23 g/mol) and $n$ = number of main-chain bonds in the chain repeating unit (in our case $n$ = 2). This resulted in a theoretical maximum grafting density of $\sigma_{Theo}$ = 0.58 chains/nm$^2$ which is in good agreement with the experimental results. The polydispersity of the bulk polymer slightly increased from 1.3 to 1.6 when the molecular weight was increased from $M_n$ = 14 700 g/mol to 55 300 g/mol. Compared to the polydispersity of the bulk PVBPT, even at molecular weights above 50 000 g/mol, the polymerization takes place under more controlled conditions (Supporting Information, Table T 3). Therefore, we assume that the polymer film surface should be more homogeneous compared to PVBPT grafted brush polymer film.

After grafting AE brushes to ITO substrate, in a second step, we functionalized the active ester groups with the moieties NMB and MPMA according to Scheme 3. In order to get rid of the nonreacted moieties, the substrates were extracted thoroughly with a good solvent. In order to show the successful attachment of the moieties to the AE brushes, UV/vis

**Scheme 3. Postfunctionalization of Poly-DPVB Activated Ester Brushes with NMB and MPMA**

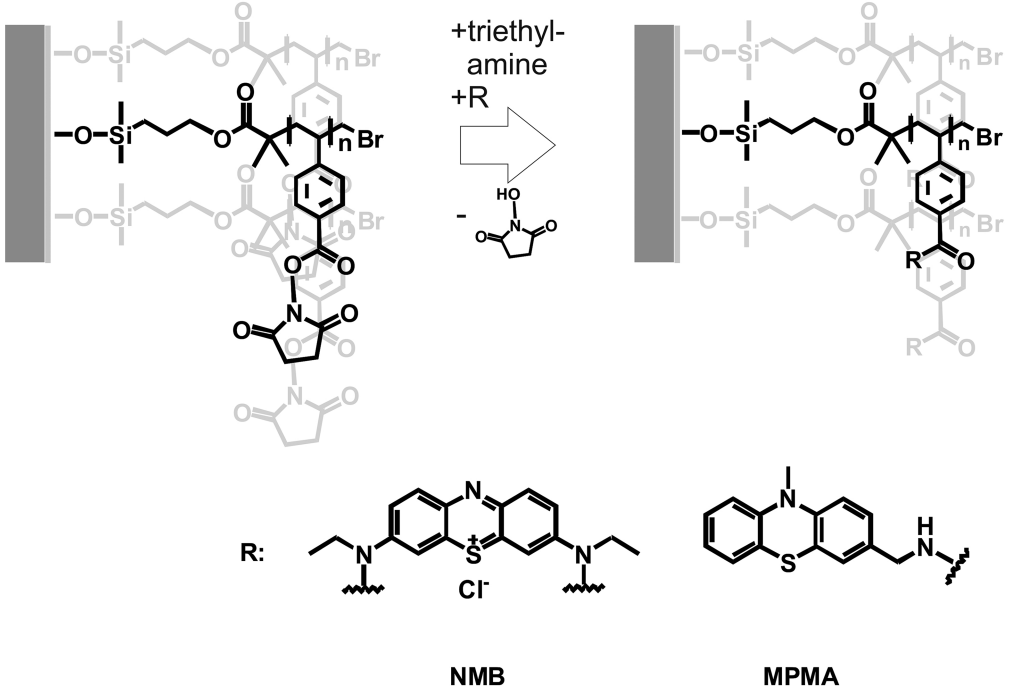


measurements were performed on grafted brushes before and after the functionalization with NMB and MPMA (for brush thickness of 26.3 nm). For both cases, a successful attachment of the moieties with the AE brush was observed. However, the reaction apparently did not take place quantitatively (Supporting Information, Figure S 10).

**Redox Functionality of Functionalized AE Grafted Brushes.** To check the functionality, i.e., the redox activity of postfunctionalized AE brushes, CV measurements were performed in solution (Figure 4). The CV data showed no oxidation peak for the AE brushes before functionalization (Figure 4a, AE on ITO). For the first experiment, ITO substrates with AE brushes postfunctionalized with NMB were measured against Ag/AgCl. After modification with NMB, we observed an anodic oxidation peak at $E_0^{0/+1}$ = 0.48 V and a cathodic reduction peak of $E_0^{+1/0}$ = 0.35 V at a scan speed of 10 mV/s (Figure 4a, AE + NMB). By increasing the scan speed up to 50 mV/s, the oxidation peak slightly shifted to $E_0^{0/+1}$ = 0.56 V, respectively. Simultaneously, the reduction peak shifted to $E_0^{+1/0}$ = 0.28 V. The free NMB revealed an oxidation peak at $E_0^{0/+1}$ = 0.34 V and a reduction peak at $E_0^{+1/0}$ = 0.19 V with a scan speed of 10 mV/s (Supporting Information, Figure S 11). The sweep cycle could be repeated for more than 10 times without any significant change in the position and intensity of the peaks.

The increased stability indicates that the moieties have been integrated inside the polymer brush matrix. The peak separation between free NMB and NMB grafted to AE brushes was $\Delta E_0$ = 0.15 and 0.13 V, respectively. The shifts in the peak position for free NMB and grafted NMB (around 140 mV) might result from the overpotential at the ITO working electrode. The increased diffusion barrier at the polymer film/ITO interface could lead to an increase of the oxidation potentials. From the integral below the CV curves, we estimated the conversion degree of the AE brushes with NMB. For a known concentration of 0.1 mM NMB in acetonitrile, we obtained an integral of $1.68 \times 10^{-5}$ $\mu$AV/cm$^2$ in the range of −0.14 and 0.66 V. For the NMB grafted to the AE brushes, an integral of $5.87 \times 10^{-7}$ $\mu$AV/cm$^2$ (range 0 to 0.8 V, shifted around the oxidation peak) was observed which corresponds to $7.49 \times 10^{-9}$ mol NMB. Taking the molecular

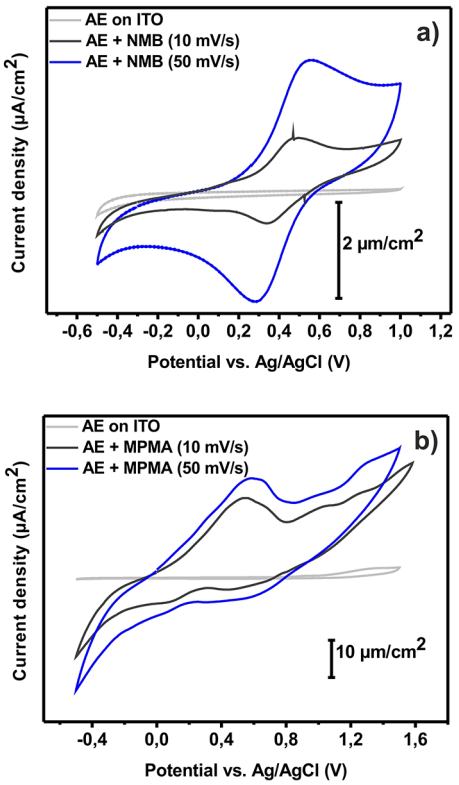


**Figure 4.** Cyclic voltammetry of grafted AE brush on ITO substrate at different scan speeds in 0.1 M tetrabutylammonium perchlorate/acetonitrile solution before and after reaction with (a) NMB and (b) MPMA. The potential is measured with Ag/AgCl and Pt as the reference and the counter electrode, respectively.


dx.doi.org/10.1021/am302869d | ACS Appl. Mater. Interfaces 2013, 5, 2485−2494

weight of $M_n$ = 55 300 g/mol and the grafting density of $\sigma_{Exp}$ = 0.36 chains/nm$^2$ of AE brushes into account, 1.43 × 10$^{-8}$ mol of activated ester groups are available on an ITO substrate of 1.21 cm$^2$ size. This means that almost 52% of the active sites have been replaced by NMB. Thus, the reaction with NMB did not proceed quantitatively. However, we have to consider that NMB has two amine functionalities which might react with the activated ester groups. Therefore, the conversion degree can only be considered as a rough estimation. This observation can be explained by the hindered diffusion of the moiety through the polymer film. In the reaction solvent DMF, the AE brushes are slightly swollen.[59] However, due to the bulkiness of NMB and its hydrophilic nature, NMB cannot completely penetrate the polymer film. For thinner AE brush films, we found that more activated ester moieties can be converted with NMB. For AE brush films with 7.9 nm thickness, a conversion degree of 82% was determined via CV measurements after the reaction with NMB (Supporting Information, Figure S 12).

For the second experiment, AE brushes with the same thickness on ITO were postfunctionalized with MPMA (Figure 4b). After the modification with MPMA, an anodic oxidation peak at $E_0^{0/+1}$ = 0.58 V and a cathodic reduction peak at $E_0^{+1/0}$ = 0.45 V were measured at a scan speed of 10 mV/s (Figure 4b, AE + MPMA). At the scan speed of 50 mV/s, the oxidation peak shifted to $E_0^{0/+1}$ = 0.62 V and the reduction peak is hardly to be distinguished, since the minimum is situated in a plateau region (approximately at $E_0^{+1/0}$ = 0.35 V). The free MPMA showed an oxidation peak at $E_0^{0/+1}$ = 0.54 V and a reduction peak at $E_0^{+1/0}$ = 0.43 V with a scan speed of 10 mV/s (Supporting Information, Figure S 13). The peak separation between free MPMA and MPMA grafted to AE brush was $\Delta E_0$ = 0.11 V and 0.13 V, respectively, for a scan speed of 10 mV/s. Again, we observed a shift of the oxidation potential from free MPMA and the MPMA grafted to AE brushes. This behavior can be attributed to the overpotential at the polymer/ITO interphase. The overpotential is partially related to the diffusion process to the electrode. Irregularities in the CV curves baseline give additional hints that side reaction at the electrode interface might also contribute to the shift due to overpotential. However, the shift in this case was around 40 mV and much smaller than the shift for free NMB compared to grafted NMB (140 mV). We estimated the conversion degree of the AE brushes with MPMA from the integral below the CV curves. For a known concentration of 0.03 mM MPMA in acetonitrile, we obtained an integral of 3.97 × 10$^{-5}$ $\mu$AV/cm$^2$ in the range of −0.04 and 0.76 V. For the MPMA grafted to the AE brushes, an integral of 5.53 × 10$^6$ $\mu$AV/cm$^2$ (range 0 to 0.8 V, shifted around the oxidation peak) was observed which corresponds to 9.57 × 10$^{-9}$ mol MPMA. Taking the molecular weight of $M_n$ = 50 300 g/mol and the grafting density of $\sigma_{Exp}$ = 0.36 chains/nm$^2$ of AE brushes into account, 1.43 × 10$^{-8}$ mol of active ester groups are available on the grafted ITO of 1.21 cm$^2$ size. Thus, we obtained a conversion degree of approximately 67%. The conversion degree was around 15% higher than for NMB which can be explained by the sterical hindrance of NMB compared to MPMA. Furthermore, secondary amines are known to be less reactive than primary amines with respect to the conversion reaction with activated esters.[29]

In conclusion, both brush types showed proper redox behavior. We could estimate the conversion degree of the AE brushes with the moieties NMB and MPMA from the CV measurements. The conversion did not complete quantitatively. This result is good agreement with our previous assumption from the UV/vis data. However, thinner AE brush films revealed higher conversion degrees compared to thicker films. Diffusion of the moieties through the thin polymer film is obviously easier. Thus, more moieties can react with the AE units. To get a better insight into the conversion reaction of the moieties with activated ester and to characterize the surface morphology of the redox active AE brushes, surface analysis methods were performed.

**Surface Analysis of AE Brushes.** To examine the surface morphology, we imaged the surface topography of the AE brushes with SFM before and after the reaction with the redox moieties NMB and MPMA. The SFM images proved the formation of a very homogeneous AE brush film before the reaction (Supporting Information, Figure S 14). From the SFM topography image, a RMS roughness ranging between 0.3 and 0.7 nm was determined. The surface RMS roughness measured with XRR varied between 0.6 and 0.9 nm independent of the molecular weight (See Supporting Information, Table T3). The results from the RMS roughness are in good accordance with the SEC data. Compared to PVBPT grafted brushes, the AE brushes resulted in more homogeneous films and revealed almost no agglomerations of polymers. Thus, a low polydispersity of the free polymer corresponds to increased homogeneity of the polymer brush film. The surface properties of the NMB and MPMA postfunctionalized AE brushes were examined with SFM (Figure 5). Before the reaction, the surface

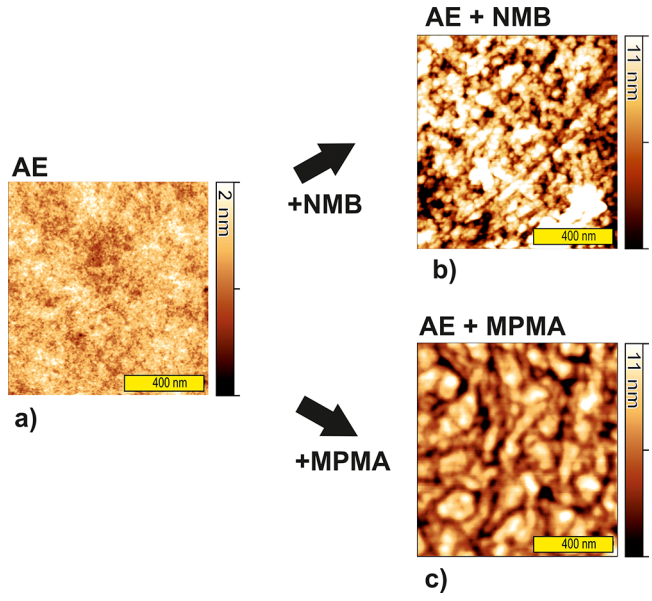


**Figure 5.** (a) Topography image of grafted AE brush (brush thickness 26.3 nm) on Si. Topography image of grafted AE brush on Si after the postfunctionalization (b) with NMB (c) and with MPMA.

topography of the AE brushes exhibited a RMS roughness of 0.3 nm (Figure 5a). However, the RMS roughness increased up to 4.3 and 2.4 nm after the reaction with NMB (Figure 5b) and MPMA (Figure 5c), respectively. We assume that the increase of the RMS roughness is related to the reaction of the moieties with AE brush which changes the chemical properties of the polymer brush.

Furthermore, in the case of NMB postfunctionalized brushes, the RMS roughness calculated from XRR data increased with the thickness of the initial AE brush from 0.9 to 5.7 nm by increasing the thickness from 7.9 to 30.3 nm, respectively

(Supporting Information, Figure S 15 and Table T 4). The RMS roughness measured by the SFM, showed a similar increase of the RMS of 2.0 to 4.3 nm, respectively (Supporting Information, Figure S 15 and Table T 4). The thicker the AE brush film, the more significant were the changes in the polymer film RMS roughness and morphology after the functionalization. This increase in the RMS roughness can be explained by the phase separation that takes place at higher molecular weights.[60] Since the reaction proceeds more slowly and less conversion takes place, the grafting density (here in terms of postfunctionalizing the activated ester moieties) decreases. Postfunctionalized regions form larger domains which tend to phase separate.

In addition, XPS measurements of AE brushes before and after the reaction with NMB and MPMA were performed (Supporting Information, Figure S 16). In particular, we have analyzed the carbon peak before and after the reaction with NMB and MPMA (Figure 6). We deduced that the ester bond

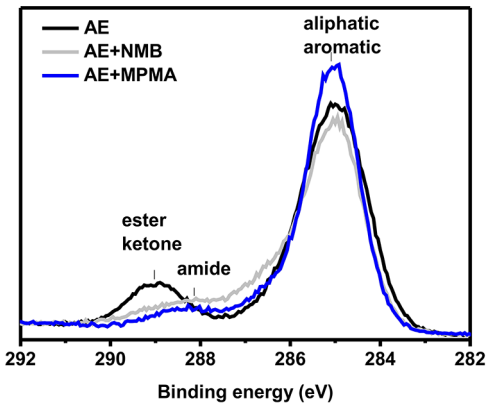


**Figure 6.** XPS spectra of the carbon ($C_{1s}$) peak from grafted AE brush on silicon substrate before and after functionalization with NMB and MPMA.

of the activated ester brushes at around 289 eV widely disappears and shifts to a new bound at around 288 eV which can be related to the amide bond formation. The aromatic and aliphatic signals appeared as a broad peak at around 285 eV. However, the broadening of the carbon peak at 288 eV indicates that some activated ester moieties did not react. From the ratio between the elements, we could confirm the successful reaction of both moieties NMB and MPMA with the AE brushes (Supporting Information, Tables T 5–T 7). In both cases, the amount of carbon increased while the amount of oxygen decreased simultaneously. Additionally, the sulfur content increased which shows the attachment of the sulfur containing dyes. Furthermore, we discovered that there is no corresponding zinc peak for NMB. The $ZnCl_2$ of NMB double salt must have been washed away after the reaction and subsequent extraction. The absence of $ZnCl_2$ is a further proof that NMB has reacted successfully with the brush moieties. According to the XPS results, we assume the polymer brush film is rather cross-linked by attachment of two amine groups rather than only one amine group (Supporting Information, Table T 6).

In the following step, the mechanical stability was investigated. The RMS roughness of the topography images decreased slightly from 2.8 to 2.5 nm after 100 scans in contact mode with an applied load of 10 nN. The scanned area showed a smoother surface after the nanowear experiment. Only a small amount of piled up material (~1–2 nm increase) was visible in the left edge of the line profile. This pile up arises from loose impurities on the surface. The nanowear experiment for the MPMA postfunctionalized brush revealed lower mechanical nanowear stability compared to NMB postfunctionalized brushes (Figure 7b). The RMS roughness increased from 4

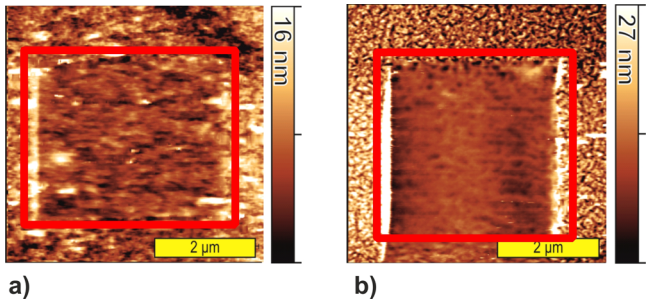


**Figure 7.** Nanowear experiment of AE brushes on ITO substrate after the reaction with NMB and MPMA at 10 nN with the speed of 50 μm/s (marked with a square). The topography was imaged after the wear experiment. (a) Topography image for NMB postfunctionalized AE brushes. (b) Topography image for MPMA postfunctionalized AE brushes.

to 7.3 nm after the nanowear test. At the edge of the scanned area, a strong pile up of the surface is visible. The difference between the nanowear stability of the NMB and MPMA functionalized brushes can be explained by the cross-linking ability of the redox moieties. MPMA has only one amine functional group. Therefore, it is not possible to form cross-linking between the brush chains. NMB however has two secondary amine groups and can function as cross-linking agent between the grafted polymer chains. This additional cross-linking leads to the formation of a polymer network, which is then mechanically more stable. Berger et al.[11] reported on an increase of wear stability for cross-linked plasma polymers and cross-linked polycarbonates compared to noncross-linked ones using SFM nanowear experiments. The increase of the elastic modulus is the reason for the high stability of cross-linked polymer brushes, since the polymer film is less penetrated due to the cross-linking.[61]

## SUMMARY AND CONCLUSION

In this work, we could successfully establish two different approaches for synthesizing redox active polymer brushes with phenothiazine moieties. We found out that both approaches are feasible and have their advantages as well as disadvantages. Polymer brushes with phenothiazine moieties on each repetition unit were successfully attached to a conducting ITO substrate using direct polymerization via SI-ATRP. The so formed brushes revealed redox behavior on the surface. In addition, the obtained polymer brush surfaces showed an increased mechanical stability during the nanowear experiments. The synthesis of PVBPT and the direct polymerization technique were both performed as a single step reaction which is desirable with respect to the synthetic expense. The direct polymerization of monomers with phenothiazine redox moieties is interesting for obtaining redox active surfaces. However, the surface morphology revealed inhomogeneities due to agglomerate formation. Better control over the polymerization reaction can be achieved by addition of deactivating species to the ATRP solution or by controlling

the reaction via activator generated by electron transfer (AGET).[62] Homogeneous surfaces with high grafting densities are desirable for SFM based data storage. On homogeneous surfaces, the topography has less influence on the scanning process during writing and reading in contact mode. By improving the reaction conditions, the formation of the agglomerates might be suppressed. Other phenothiazine containing monomers with higher reactive backbones such as acrylates can be used instead.

The activated ester approach resulted in homogeneous polymer brush films. Therefore, the approach with activated ester is a more promising technique for synthesizing redox active surfaces for SFM based data storage. We synthesized grafted activated ester brushes with succinimide moieties using SI-ATRP. Compared to PVBPT grafted brushes, the grafting density could be slightly increased by using activated ester brushes. A higher grafting density means more redox moieties in the patterned area which can help to increase the storage density. These brushes were then functionalized in the second step using the moieties NMB and MPMA. Both moieties reacted with the activated ester brush, which was proved using various techniques such as UV/vis, CV, and XPS. From these data, we concluded that the reaction did not take place quantitatively. Since the conversion of the moieties with the activated brush polymer units was not quantitative, phase separation took place. Therefore, the RMS roughness of the polymer film increased depending on the film thickness and on the moiety. Thinner films proved to show less increase of the RMS roughness. Due to facile diffusion of the redox moieties through the polymer brush film, thinner films exhibited increased reactivity. We observed that the size of the moiety also plays a role for the postfunctionalization. Apparently, MPMA is sterically less hindered and resulted in higher conversion of the activated ester moieties than NMB. With respect to nanowear stability, activated ester brushes showed differences depending on the degree of cross-linking with the redox moiety. NMB functionalized brushes exhibited a higher nanowear resistance than MPMA functionalized brushes. As expected, the additional cross-linking using NMB as the redox moiety resulted in more stable surfaces. With the postfunctionalization technique, nanowear stable redox active polymer brushes can easily be synthesized. To improve the conversion reaction, more reactive amine moieties should be used. Especially, primary amine groups are more reactive species compared to secondary amines. The film thickness is an important factor as well. Low film thickness facilitates the diffusion of the redox moieties and enables the reaction with the activated ester groups. With variation of monomer and moieties, nanowear stable redox surfaces can be obtained on almost every type of substrate for potential application in the textile and electronic industries.

## ■ ASSOCIATED CONTENT

### Supporting Information

Synthetic approach to VBPT, AE monomer DPVB, MPMA, grafting from polymer brushes via ATRP and postfunctionalization of AE polymer brushes; XRR curves of grafted polymers surface for PVBPT and AE before and after functionalization, contact angle images of PVBPT grafting process, SEC results and film thickness dependency for PVBPT and AE; MD-simulation of grafted PVBPT brush; XPS spectra, SFM topography map of grafted polymer surface for PVBPT and AE before and after functionalization; XPS quantitative calculations for grafted polymer surface for PVBPT and AE before and after functionalization; UV/vis for grafted polymer surface of AE before and after functionalization; CV results for PVBPT in solution, AE brush modified with MPMA, pure NMB, and MPMA. This information is available free of charge via the Internet at http://pubs.acs.org/.

## ■ AUTHOR INFORMATION

### Corresponding Author

*E-mail: jochen.gutmann@uni-due.de.

### Notes

The authors declare no competing financial interest.

## ■ ACKNOWLEDGMENTS

This project was partially supported by the Strategic Japanese German 756 Cooperative Programme On Nanoelectronics (BE3286/2-1; 757 GU 771/6-1), Japanese science and Technology founding, International Research Training Group 1404 "Self-organized Materials for Optoelectronics" (DFG), and the European Research Council under the project ProTem. The authors would like to thank Jürgen Ziegler from the Center of Smart Interfaces in Darmstadt, Germany for the XPS measurements. Furthermore, Gunnar Kircher, Masaya Toda, Akiko Itakura, Uwe Rietzler, Sandra Seywald, and Markus Mezger are thanked for their help with the synthesis and measurements. The authors acknowledge countrywide license for Accelrys Materials Studio (ICM, Univ. Warsaw) provided by Wroclaw Centre for Networking and Supercomputing through the grant number 150.

## ■ REFERENCES

(1) Ling, Q. D.; Liaw, D. J.; Zhu, C.; Chan, D. H.; Kang, E. T.; Neoh, K. G. *Prog. Polym. Sci.* **2008**, *33*, 917−978.
(2) Nishide, H.; Suga, T. *Electrochem. Soc. Interface* **2005**, *14*, 32−38.
(3) Reiter, G. *Phys. Rev. Lett.* **1992**, *68*, 75−78.
(4) Yang, X.; Loos, J. *Macromolecules* **2007**, *40*, 1353−1362.
(5) Arnold, R. M.; Huddleston, N. E.; Locklin, J. *J. Mater. Chem.* **2012**, *22*, 19357−19365.
(6) Kessler, D.; Jochum, F. D.; Choi, J.; Char, K.; Theato, P. *Appl. Mater. Interfaces* **2011**, *3*, 124−128.
(7) Günay, K. A.; Schüwer, N.; Klok, H.-A. *Polym. Chem.* **2012**, *3*, 2186−2192.
(8) Alexander, S. *J. Phys. (Paris)* **1977**, *38*, 977−981.
(9) De Gennes, P. G. *Macromolecules* **1980**, *13*, 1069−1075.
(10) Milner, S. T. *Science* **1991**, *251*, 905−914.
(11) Berger, R.; Cheng, Y.; Förch, R.; Gotsmann, B.; Gutmann, J. S.; Pakula, T.; Rietzler, U.; Schärtl, W.; Schmidt, M.; Strack, A.; Windeln, J.; Butt, H. J. *Langmuir* **2007**, *23*, 3150−3156.
(12) Bhushan, B.; Kwak, K. J.; Palacio, M. *J. Phys.: Condens. Matter* **2008**, *20*, 365207/1−365207/34.
(13) Tranchida, D.; Sperotto, E.; Chateauminois, A.; Schönherr, H. *Macromolecules* **2011**, *44*, 368−374.
(14) Gotsmann, B.; Knoll, A. W.; Pratt, R.; Frommer, J.; Hedrick, J. L.; Duerig, U. *Adv. Funct. Mater.* **2010**, *20*, 1276−1284.
(15) Lee, M. H.; Hwang, C. S. *Nanoscale* **2011**, *3*, 490−502.
(16) Gotsmann, B.; Duerig, U. T.; Sills, S.; Frommer, J.; Hawker, C. J. *Nano Lett.* **2006**, *6*, 296−300.
(17) Zapotoczny, S.; Benetti, E. M.; Vancso, G. J. *J. Mater. Chem.* **2007**, *17*, 3293−3296.
(18) Nishide, H.; Oyaizu, K. *Science* **2008**, *319*, 737−738.
(19) Nishide, H.; Iwasa, S.; Pu, Y. J.; Suga, T.; Nakahara, K.; Satoh, M. *Electrochem. Acta* **2004**, *50*, 827−831.
(20) Bugnon, L.; Morton, C. J. H.; Novak, P.; Vetter, J.; Nesvadba, P. *Chem. Mater.* **2007**, *19*, 2910−2914.
(21) Oyaizu, K.; Nishide, H. *Adv. Mater.* **2009**, *21*, 2339−2344.

(22) Ibe, T.; Frings, R. B.; Lachowicz, A.; Kyo, S.; Nishide, H. *Chem. Commun.* **2010**, *46*, 3475−3477.
(23) Kojima, K.; Nakahira, T.; Honzawa, K.; Iwabuchi, S. *Macromol. Rapid Commun.* **1986**, *7*, 365−368.
(24) Wang, Y. H.; Hung, M. K.; Lin, C. H.; Lin, H. C.; Lee, J. T. *Chem. Commun.* **2011**, *47*, 1249−1251.
(25) Tu, H.; Heitzman, C. E.; Braun, P. V. *Langmuir* **2004**, *20*, 8313−8320.
(26) Matyjaszewski, K.; Xia, J. *Chem. Rev.* **2001**, *101*, 2921−2990.
(27) Barbey, R.; Lavanant, L.; Paripovic, D.; Schüwer, N.; Sugnaux, C.; Tugulu, S.; Klok, H. A. *Chem. Rev.* **2009**, *109*, 5437−5527.
(28) Pyun, J.; Matyjaszewski, K. *Chem. Mater.* **2001**, *13*, 3436−3448.
(29) Nilles, K.; Theato, P. *Eur. Polym. J.* **2007**, *43*, 2901−2912.
(30) Roth, P. J.; Wiss, K. T.; Zentel, R.; Theato, P. *Macromolecules* **2008**, *41*, 8513−8519.
(31) Yakushiji, T.; Sakai, K.; Kikuchi, A.; Aoyagi, T.; Sakurai, Y.; Okano, T. *Langmuir* **1998**, *14*, 4657−4662.
(32) Choi, J.; Schattling, P.; Jochum, F. D.; Pyun, J.; Char, K.; Theato, P. *J. Polym. Sci.* **2012**, *50*, 4010−4018.
(33) Kessler, D.; Metz, N.; Theato, P. *Macromol. Symp.* **2007**, *254*, 34−41.
(34) Theato, P. *J. Polym. Sci.* **2008**, *46*, 6677−6687.
(35) Golriz, A. A.; Kaule, T.; Heller, J.; Untch, M. B.; Schattling, P.; Theato, P.; Toda, M.; Yoshida, S.; Ono, T.; Butt, H. J.; Gutmann, J. S.; Berger, R. *Nanoscale* **2011**, *3*, 5049−5058.
(36) Jelinek, I.; Nemcova, I.; Rychlovsky, P. *Talanta* **1991**, *38*, 1309−1313.
(37) Shine, H. J.; Mach, E. E. *J. Org. Chem.* **1965**, *30*, 2130−2139.
(38) Iida, Y. *Bull. Chem. Soc. Jpn.* **1972**, *44*, 663−667.
(39) Morishima, Y.; Akihara, I.; Nozakura, S. I. *J. Polym. Sci.* **1985**, *23*, 661−663.
(40) Son, S. K.; Choi, Y. S.; Lee, W. H.; Hong, Y.; Kim, J. R.; Shin, W. S.; Moon, S. J.; Hwang, D. H.; Kang, I. N. *J. Polym. Sci.* **2010**, *48*, 635−646.
(41) Parratt, L. G. *Phys. Rev.* **1954**, *95*, 359−369.
(42) Ell, J. R.; Mulder, D. E.; Faller, R.; Patten, T. E.; Kuhl, T. L. *Macromolecules* **2009**, *42*, 9523−9527.
(43) Privalko, V. P. *Macromolecules* **1980**, *13*, 370−372.
(44) Kimura, A.; Yoshimoto, S.; Akano, Y.; Hirata, H.; Kusabayashi, S.; Mikawa, H.; Kasai, N. *J. Polym. Sci.* **1970**, *8*, 643.
(45) Morishima, Y.; Akihara, I.; Lim, H. S.; Nozakura, S. *Macromolecules* **1987**, *20*, 978−983.
(46) Laglera, L. M.; van den Berg, C. M.G. *Mar. Chem.* **2003**, *82*, 71−89.
(47) Ingall, M. K.; Honeyman, C. H.; Mercure, J. V.; Bianconi, P. A.; Kunz, R. R. *J. Am. Chem. Soc.* **1999**, *121*, 3607−3613.
(48) Vallant, T.; Brunner, H.; Mayer, U.; Hoffmann, H.; Leitner, T.; Resch, R.; Friedbacher, G. *J. Phys. Chem. B* **1998**, *102*, 7190−7197.
(49) Matyjaszewski, K.; Miller, P. J; Shukla, N.; Immaraporn, B.; Gelman, A.; Luokala, B. B.; Siclovan, T. M.; Kickelbick, G.; Vallant, T.; Hoffmann, H.; Pakula, T. *Macromolecules* **1999**, *32*, 8716−8724.
(50) Aoike, T.; Uehara, H.; Yamanobe, T.; Komoto, T. *Langmuir* **2001**, *17*, 2153−2159.
(51) Meyers, G. F.; DeKoven, B. M.; Seitz, J. T. *Langmuir* **1992**, *8*, 2330−2335.
(52) Pihan, S. A.; Emmerling, S. G.; Butt, H. J.; Gutmann, J. S.; Berger, R. *Wear* **2011**, *271*, 2852−2856.
(53) Aamer, K. A.; Tew, G. N. *J. Polym. Sci.* **2007**, *45*, 5618−5625.
(54) Son, W. G.; Kim, J.; Seo, J. P.; Yoon, J.; Choi, M.; Lee, L. Y.; Lee, I. *Vet. Anaesth. Analg.* **2011**, *38*, 510−515.
(55) Matyjaszewski, K.; Davis, T. P. *Handbook Of Radical Polymerization*; Wiley-Interscience: New York, 2002; pp 523.
(56) Haddleton, D. M.; Crossman, M. C.; Hunt, K. H.; Topping, C.; Waterson, C.; Suddaby, K. G. *Macromolecules* **1997**, *30*, 3992−3998.
(57) Orski, S. V.; Fries, K. H.; Sheppard, G. R.; Locklin, J. *Langmuir* **2010**, *26*, 2136−2143.
(58) Ramakrishnan, A.; Dhamodharan, R.; Rühe, J. *Macromol. Rapid Commun.* **2002**, *23*, 612−616.
(59) Bumbu, G. G.; Wolkenhauer, M.; Kircher, G.; Gutmann, J. S.; Berger, R. *Langmuir* **2007**, *23*, 2203−2207.
(60) Siqueira, D. F.; Kohler, K.; Stamm, M. *Langmuir* **1995**, *11*, 3092−3096.
(61) Torres, J. M.; Stafford, C. M.; Vogt, B. D. *ACS Nano* **2010**, *4*, 5357−5365.
(62) Jakubowski, W.; Matyjaszewski, K. *Macromolecules* **2005**, *38*, 4139−4146.